Non-immunogenic and reversible transgene expression using self-amplifying RNA

Tony K.Y. Lim*, Anne Ritoux, Luke W. Paine, Larissa Ferguson, Tawab Abdul, Ewan St. John Smith*

*Corresponding authors

Abstract

Current self-amplifying RNA (saRNA) vectors induce apoptosis and inflammation, restricting their therapeutic potential. By engineering saRNA to co-express viral and cellular inhibitors that target multiple innate immune pathways, we achieve reversible transgene expression while minimizing cytotoxicity and immunogenicity. This advancement enables broader applications for saRNA beyond vaccines, creating opportunities for non-inflammatory RNA-based therapeutics with sustained and reversible transgene expression.

Main

Self-amplifying RNA (saRNA) technology, with two approved vaccines now in clinical use, has shown significant potential in vaccine development[1]. Upon cellular internalization, saRNA utilizes host machinery to synthesize an RNA-dependent RNA polymerase (RdRp)[2]. This RdRp generates a negative-strand RNA intermediate, serving as a template for both genomic and subgenomic RNA production[3]. The subgenomic RNA encodes the gene of interest and is transcribed in excess of the genomic RNA, leading to robust and sustained protein expression[4].

While saRNA's self-replication mechanism enables sustained protein expression, it also activates cytosolic double-stranded RNA (dsRNA) sensors which results in suppression of cap-dependent translation[5], RNA degradation[6], apoptosis[7], and induction of proinflammatory cytokines and chemokines[8]. While this inherent immunogenicity enhances saRNA's efficacy as a vaccine[9], it hinders its use as a therapeutic in contexts where innate immune activation is undesirable, such as protein replacement therapy, therapeutic antibody production, genome editing, cellular reprograming and immune cell engineering.

To address these challenges, we developed a fully saRNA-based approach that inhibits multiple innate immune pathways using viral and cellular inhibitors. Viruses have evolved mechanisms to evade host immune responses, and co-expression of viral innate immune inhibitory proteins has shown promise in reducing saRNA immunogenicity[10]. Previous studies used cap-dependent translation for inhibitory protein co-expression[11–13], a process suppressed by innate immune responses. We hypothesized that inhibiting multiple dsRNA sensing pathways with cap-independently expressed proteins could enable prolonged saRNA expression without excessive immune activation.

We tested this hypothesis by designing saRNA constructs incorporating both cap-dependent and cap-independent translation systems (Fig. 1a). These constructs express EGFP via internal ribosome entry site (IRES)-mediated translation and mScarlet3 via subgenomic cap-dependent

translation, allowing assessment of translational control. The saRNA also includes non-structural proteins (nSP) 1-4 from the Venezuelan equine encephalitis virus (VEEV), which form the RdRp used to replicate the saRNA. We engineered constructs encoding either moxBFP or viral innate immune inhibitors through IRES translation: one expressing Vaccinia virus E3 protein (a pleiotropic inhibitor of dsRNA sensing)[14], and another combining E3 with Toscana virus NSs protein (ubiquitin ligase for protein kinase R [PKR])[15] and Theiler's virus L* protein (RNase L inhibitor)[16] to further suppress PKR and the oligoadenylate synthase (OAS)/RNase L pathways.

We used mouse primary fibroblast-like synoviocytes (FLS) (Supplementary Fig. 1) as our target cell type, given their key role in arthritic joint diseases[17,18]. FLS were labeled with BioTracker NIR680, a lipid membrane dye. Mock transfection using Lipofectamine MessengerMAX increases BioTracker fluorescence compared to non-transfected cells. Inducing apoptosis with staurosporine decreased BioTracker fluorescence, indicating reduced cell numbers (Supplementary Fig. 2a,b). BioTracker results aligned with those from the viability dye calcein AM (Supplementary Fig. 2c,d). Following transfection of saRNA constructs, we monitored BioTracker, EGFP, and mScarlet3 fluorescence over 3 weeks (Fig. 1b,c). Spectral overlap between EGFP and mScarlet3 was corrected using linear unmixing (Supplementary Fig. 3a,b).

Transfection with native (moxBFP-encoding) saRNA (i.e. lacking immune inhibitors), induced immediate and long-term cytotoxicity. Co-expression of E3 initially preserved cell viability, though it gradually diminished over time. However, the E3-NSs-L* construct produced more sustained protection against the decline in cell viability (Fig. 1d). These findings were corroborated using both the cell number normalization stain CellTag and calcein AM (Supplemental Fig. 4a,b).

Viral innate immune inhibiting proteins significantly enhanced saRNA-driven protein expression. E3 co-expression produced the highest levels of EGFP and mScarlet3 fluorescence, surpassing both native saRNA and the E3-NSs-L* construct (Fig. 1e,f). Native saRNA alone yielded low protein levels, while E3-NSs-L* showed intermediate expression. These results indicate that E3 most effectively augments saRNA expression, but at the cost of reduced cell viability.

A longitudinal apoptosis assay using Annexin-V (A5) staining revealed distinct cytotoxicity patterns. Staurosporine, serving as a positive control, caused a temporary increase in A5 staining, which diminished after the cells underwent apoptosis. Native saRNA significantly increased A5 staining in the first two days, while E3 showed a delayed but persistent increase from day 2 onward (Fig. 1g,h). In contrast, E3-NSs-L* did not significantly affect A5 staining, indicating reduced cytotoxicity. These patterns aligned with the observed changes in BioTracker fluorescence.

We then examined how viral innate immune inhibitors affected translational control mechanisms. In-cell western assays showed that native saRNA increased eIF2α phosphorylation, which was significantly reduced by co-expression of either E3 or E3-NSs-L* (Fig. 1i). Since PKR mediates eIF2α phosphorylation, we next examined PKR levels and found that they increased following saRNA transfection, but this was significantly reduced with co-expression of E3-NSs-L* (Fig. 1j). Notably, the E3-NSs-L* construct, unlike E3 alone, also led to a significant increase in total eIF2α levels (Supplementary Fig. 5a). We also investigated eIF4E, another key player in translational regulation. saRNA transfection induced dephosphorylation of eIF4E without affecting its total levels (Supplementary Fig. 5b,c); co-expression of E3 or E3-NSs-L* did not influence these changes in eIF4E.

Although E3-NSs-L* saRNA both prevents saRNA-induced eIF2α phosphorylation (Fig. 1i) and increases total eIF2α availability for cap-dependent initiation (Supplementary Fig. 5a), it paradoxically resulted in lower mScarlet3 expression compared to the E3 construct (Fig. 1f). The E3 construct also produced extremely high levels of EGFP expression (Fig. 1e), which is surprising since translation suppression was not induced by this construct. A likely explanation is that saRNA replication activates OAS, leading to RNase L activation and degradation of cellular mRNA. Reduced cellular mRNA levels would free up more ribosomes for saRNA translation, a process blocked by Theiler's virus L*, which inhibits RNase L[16].

Supporting this hypothesis, cells transfected with E3-NSs-L* showed higher RNA integrity than those with E3 alone (Fig. 1k). The inhibition of activated RNase L by Theiler's virus L* also explains the reduced cytotoxicity observed with the E3-NSs-L* construct compared to E3 (Fig. 1d).

Having mitigated saRNA-induced toxicities such as translational shutoff, RNA degradation, and apoptosis, we next focused on addressing saRNA-induced cytokine production. We created constructs expressing E3-NSs-L*-EGFP via one IRES, and either moxBFP or cellular inhibitors of inflammatory signaling via another IRES (Fig. 2a). Given that nuclear factor-κB (NF-κB) is a hallmark of viral infection and a master regulator of pro-inflammatory cytokine and chemokine induction,[19,20] we targeted its inhibition using super repressor inhibitor of κBα (srIκBα). This dominant active form of IκBα cannot be phosphorylated and thus resists ubiquitination and degradation, forming a stable cytoplasmic pool that prevents NF-κB nuclear translocation[21,22]. We generated a construct expressing srIκBα alone, and another expressing srIκBα in combination with Smad7 and suppressor of cytokine signaling (SOCS1). Smad7 negatively regulates both transforming growth factor-β (TGF-β) and NF-κB signaling pathways[23], while SOCS1 inhibits type I and II interferon pathways in addition to NF-κB signaling[24,25].

Using a bead-based immunoassay on FLS culture supernatant, we found that native saRNA transfection was highly immunostimulatory and induced cytokine secretion, whereas srIκBα co-expression reduced all cytokine levels, such that they were statistically insignificant from mock transfected FLS (Fig. 2b). E3 co-expression reduced TNF-α, interferon-α, and -β levels, while E3-NSs-L* co-expression additionally reduced CXCL10 levels (Fig. 2b); the srIκBα-Smad7-SOCS1 construct showed no additional cytokine inhibitory effects compared to srIκBα alone.

We then examined the effects of inhibiting inflammatory signaling on cell viability and transgene expression (Fig. 2c,d). Interestingly, the srIκBα construct reduced cell viability, while the srIκBα-Smad7-SOCS1 construct exhibited a viability profile similar to mock transfection (Fig. 2e). CellTag and calcein AM staining corroborated negative effects of srIκBα on cell viability (Supplementary Fig. 6a,b). All three constructs produced low levels of EGFP expression following transfection (Fig. 2f). However, the srIκBα-Smad7-SOCS1 construct exhibited 2- to 3-fold higher mScarlet3 fluorescence compared to the moxBFP and srIκBα constructs (Fig. 2g).

Surprisingly, co-expression of srIκBα resulted in eIF2α dephosphorylation (Supplementary Fig. 7a) and eIF4E depletion (Fig. 2h), effects not observed with srIκBα-Smad7-SOCS1. Total eIF2α levels and eIF4E phosphorylation were unchanged by either construct (Supplementary Fig. 7b,c). These results suggest that, in addition to reduced cell viability, depletion of eIF4E mediates the low transgene expression observed with the srIκBα construct.

Given that viral infection is known to drive inflammatory fibroblast activation[26,27], we investigated whether prolonged saRNA transfection could have a similar effect on FLS. We examined fibroblast activation factor-α (FAPα), a protein involved in joint destruction that is typically expressed at low basal levels in FLS but upregulated upon inflammatory activation[28–30]. Notably, FAPα levels at day 11 post-transfection were lower than mock transfection and significantly reduced by srIκBα-Smad7-SOCS1 co-expression (Fig. 2i). These findings suggest that long-term anti-inflammatory saRNA transfection not only avoids activating FLS but may also serve as an effective strategy to downregulate FAPα expression, which could be advantageous in arthritis therapy[31].

Finally, we evaluated the reversibility of srIκBα-Smad7-SOCS1 saRNA transfection. ML336[32], a small-molecule inhibitor of the VEEV RdRp used in this study, was added to the culture medium 1 day after transfection (Fig. 2j). ML336 treatment significantly reduced mScarlet3 and EGFP expression after several days (Fig. 2k, Supplementary Fig. 8a), demonstrating its effectiveness in inhibiting saRNA transfection. Notably, ML336 did not reduce cell viability, as shown by calcein AM staining, when compared to vehicle or mock transfection (Supplementary Fig. 8b).

Our findings reveal that blocking the NF-κB pathway alone is insufficient when designing anti-inflammatory saRNA constructs. While NF-κB regulates inflammation, it also plays a key role in cell surivival[33,34]. Co-expressing proteins with anti-apoptotic and pro-survival functions, such as Smad7[35,36] and SOCS1[37,38], can help counterbalance the loss of cell survival signaling resulting from NF-κB inhibition. Additionally, our study supports the known role of NF-κB signaling in reducing eIF4E levels[39] and further demonstrates that saRNA transfection induces eIF4E dephosphorylation. Although eIF4E depletion or dephosphorylation may reduce transgene expression, this effect could be harnessed for therapeutic benefit. For example, reducing eIF4E activity has been shown to decrease pain sensitivity[40], counteract tumorigenesis[41], improve neurodevelopmental social behavioral defecits[42], and promote longevity[43].

Building on our in vitro findings, the next step will be to evaluate the anti-inflammatory saRNA platform in vivo to assess its effectiveness in complex biological environments. Additionally, whereas this study utilized FLS from healthy adult mice, future research should investigate the effects of anti-inflammatory saRNA on FLS derived from disease models and its potential to modify pathological processes. Translating the anti-inflammatory saRNA platform to human cells and expanding its application to additional cell types and therapeutic contexts will also be essential for understanding its broader potential.

This study demonstrates that multi-pathway suppression of the innate immune system enables saRNA expression without cytotoxicity or excessive innate immune activation. This approach expands the therapeutic potential of saRNA, allowing for sustained, non-integrative, and reversible therapeutic transgene expression in situations where pro-inflammatory signaling is undesirable. The reversibility of this approach is particularly advantageous, as the saRNA can be removed once therapeutic objectives are achieved, thus minimizing the risk of prolonged immune suppression or other potential side effects associated with extended saRNA transfection or transgene expression.

Methods

Plasmid cloning and construct design

The commercially available TagGFP2 E3L Simplicon vector (SCR725, Merck) served as the saRNA backbone in this study. After removing the TagGFP2-IRES-E3 sequence, various constructs were generated by combining different elements using restriction digests (FastDigest, Thermo Scientific), overlap extension PCR (Phusion, Thermo Scientific), and HiFi assembly (NEBuilder, New England Biolabs).

Genetic elements were sourced as follows: mScarlet3 from pDx_mScarlet3 (a gift from Dorus Gadella [Addgene plasmid #189754])[44], IRES-EGFP from pIRES2-EGFP (Clontech), and IRES-E3 and IRES-PuroR (puromycin resistance) from the original TagGFP2 E3L Simplicon vector.

Custom gene synthesis (GeneArt, Thermo Scientific) was used to produce IRES-moxBFP, IRES-E3-T2A-NSs-P2A-L*-E2A-mEGFP, and IRES-srIκBα-P2A-Smad7-T2A-SOCS1 sequences. The IRES sequence was derived from pIRES2-EGFP (Clontech). Other sequences were derived from public databases: moxBFP (FPbase ID: SSTDU),[45] mEGFP (FPbase ID: QKFJN), E3 (UniProt: P21605-1), NSs (UniProt: P21699), L* (UniProt: P0DJX4), Smad7 (UniProt: O35253-1), and SOCS1 (UniProt: O35716). srIκBα was engineered from IκBα (UniProt: Q9Z1E3) by substituting serines 32 and 36 with alanines. All synthesized sequences were codon-optimized for mouse expression (GenSmart, GenScript).

Plasmids were cloned in DH5α competent *Escherichia coli* (High Efficiency, New England Biolabs) and purified by maxiprep (PureLink HiPure, Invitrogen). All plasmid sequences were verified using nanopore whole plasmid sequencing (Plasmidsaurus).

RNA synthesis

Plasmids were linearized using XbaI (FastDigest, Thermo Scientific) at 37°C for 3 hours. The linear plasmids were purified by phenol-chloroform extraction followed by sodium acetate ethanol precipitation. Uncapped RNA was synthesized *in vitro* using the T7 RiboMAX Large Scale RNA Production kit (Promega) at 37°C for 2 hours. After purification by ammonium acetate precipitation, the RNA was denatured at 65°C for 5 minutes. Cap-1 structures were then generated using the Vaccinia Capping System in conjunction with mRNA cap 2'-O-methyltransferase (both from New England Biolabs) for 45 minutes at 37°C. Following another ammonium acetate purification, the RNA was treated with Antarctic phosphatase (New England Biolabs) for 30 minutes at 37°C. After a final ammonium acetate purification step, the RNA was resuspended in THE RNA Storage Solution (Invitrogen), aliquoted, and stored at -80°C until use.

Animals

All mice used in this study were 5- to 12-week-old wildtype C57BL/6J mice (Envigo, Indianapolis, IN). Both male and female mice were included, though sex differences in response to saRNA transfection were not analyzed. Mice were housed in groups of up to five in a temperature-controlled room (21°C), with bedding, a red shelter, and enrichment materials provided. They were

200 maintained on a 12-hour light/dark cycle, with food and water available ad libitum. Mice were
201 euthanized by exposure to CO_2 gas in a rising concentration, and death confirmed by dislocation of
202 the atlanto-occipital joint by applying pressure to the side of the neck using thumb and forefinger,
203 procedures in line with the Animals (Scientific Procedures) Act 1986 Amendment Regulations 2012.

204

205 *Mouse primary FLS culture*

206 We cultured FLS from mouse knee joints following established protocols[46], with slight
207 modifications. In brief, knee joints were exposed by cutting through the overlying skin with
208 dissecting scissors. The patellar tendon was then grasped near the patella with Dumont tweezers,
209 and spring scissors were used to sever the patellar tendon along with surrounding tissues. Finally,
210 the patella was excised by cutting the quadriceps tendon, and excess muscle and tendons were
211 carefully trimmed away.

212 Both patellae from each animal were collected into a microcentrifuge tube containing ice-cold
213 sterile phosphate buffered saline (PBS), then transferred to a 24-well tissue culture plate (Costar)
214 with FLS culture media. The media consisted of DMEM/F-12 (Invitrogen) supplemented with 25%
215 fetal bovine serum (Sigma), 1X GlutaMAX (Gibco), and 100 µg/ml Primocin (InvivoGen).

216 The patellae were maintained in a humidified incubator at 37°C with 5% CO2, with media changes
217 every 1-2 days. FLS outgrowth was observed, and after approximately 10 days, when cells reached
218 70% confluency, the patellae were transferred to new wells for further FLS collection. Cells
219 attached to the original wells were passaged using 0.1% trypsin-EDTA (Sigma) into a single well of a
220 6-well plate (Costar). Cells were later expanded into T25 flasks (BioLite, Thermo Scientific or
221 CELLSTAR, Greiner Bio-One) and passaged upon reaching confluency. After the second passage,
222 Versene solution (Gibco) was used for cell dissociation.

223 FLS were used between passages 3 and 8. In most experiments, cells from the same animal were
224 divided and plated onto 6-well or 24-well plates, allowing for parallel manipulations with matched
225 conditions. Occasionally, when cell numbers were low, cells from different animals were pooled
226 before division. Once plated for experiments, media was changed every 2-3 days.

227

228 *Immunocytochemistry and confocal microscopy*

229 Cells were plated on poly-D-lysine-coated glass-bottom 35 mm dishes (P35GC-1.5-14-C, MatTek)
230 and fixed with 4% paraformaldehyde for 10 minutes at room temperature without permeabilization.
231 After fixation, cells were washed twice with PBS, followed by blocking with 10% normal goat serum
232 in PBS for 1 hour at room temperature.

233 Cells were then incubated overnight at 4°C in blocking buffer, either without primary antibody (no
234 primary control) or with cadherin-11 (extracellular) rabbit polyclonal antibody (1:200, DF3523,
235 Affinity Biosciences). After three washes with PBS, cells were incubated for 1 hour at room
236 temperature in blocking buffer with 1 µg/ml Hoechst 33342, BioTracker NIR680 (1:2000, Merck), and
237 goat anti-rabbit Alexa Fluor 488 secondary antibody (1:500, Invitrogen).

238 After four additional PBS washes, cells were imaged in PBS using a Leica Stellaris 5 confocal
239 microscope equipped with a 40X oil immersion objective. Tile-scanned images were stitched using
240 Las X microscopy software (Leica) to generate high-resolution panoramic images.

241

242 *BioTracker staining*

243 BioTracker NIR680 was diluted 1:2000 in unsupplemented DMEM/F-12. T25 flasks containing FLS
244 were washed once with HBSS (with calcium and magnesium, Gibco), then incubated with the
245 diluted dye for 30 minutes at 37°C. After incubation, the flasks were washed three times with FLS
246 media, with each wash lasting 10 minutes at 37°C. The FLS were then dissociated using Versene
247 and plated onto 6- or 24-well plates.

248

249 *FLS transfection*

250 For transfection in 6-well plates, the medium was removed and replaced with 1 ml of Opti-MEM I
251 (Gibco). In a microcentrifuge tube, 500 ng of saRNA was diluted in 200 µl of Opti-MEM I. In a
252 separate tube, 3 µl of Lipofectamine MessengerMAX (Invitrogen) was diluted in 100 µl of Opti-MEM
253 I. After gently mixing, the complexes were incubated at room temperature for 5 minutes, then
254 added dropwise to the cells. The cells were incubated with the complexes for 2 hours at 37°C, after
255 which the media was removed and replaced with fresh FLS media. For transfection in 24-well
256 plates, all volumes and amounts of saRNA were reduced fivefold.

257

258 *Microplate imaging*

259 Unless otherwise specified, black glass-bottom 6-well plates (P06-1.5H-N, Cellvis) were used for
260 microplate imaging. Prior to imaging, the FLS media was replaced with Live Cell Imaging Solution
261 (Invitrogen). Imaging was performed using the Odyssey M laser scanner (LI-COR), using LI-COR
262 acquisition software with a plate offset of +1.45 mm and 100 µm resolution.

263 EGFP, mScarlet3, and BioTracker NIR680 were imaged using the 488, 520, and 700 channels,
264 respectively. Spectral cross-excitation between EGFP and mScarlet3 in the 488 and 520 channels
265 was corrected through linear unmixing analysis, as described below. Fluorescence intensity was
266 quantified in ImageJ by measuring the integrated density within equal-area regions of interest for
267 each well. Fluorescence values (EGFP, mScarlet3, and BioTracker) were normalized by the day 0
268 BioTracker signal measured before transfection to account for variations in starting cell numbers.

269

270 *Linear unmixing analysis*

271 saRNA constructs encoding individual fluorescent proteins (moxBFP, EGFP, or mScarlet3) were
272 designed to assess cross-excitation among the fluorescent proteins used in this study. tSA201 cells
273 (96121229, ECACC) were seeded in black glass-bottom 6-well plates coated with poly-D-lysine
274 (Sigma) and transfected with the saRNA constructs. Cells were imaged the following day using an

275 Odyssey M laser scanner, with fluorescence captured through the 488 and 520 channels.
276 Expression of moxBFP was undetectable in both the 488 and 520 channels, and therefore it was
277 excluded from further analysis. Bleed-through of EGFP into the 520 channel and mScarlet3 into the
278 488 channel was quantified using ImageJ, with cross-excitation determined to be 11.32% and
279 0.94%, respectively. The emission signals were assumed to be linearly proportional to the sum of
280 the intensities of each fluorophore, and the unmixed EGFP and mScarlet3 signals were calculated
281 using Python.

282

283 *Annexin V assay*

284 FLS were stained with BioTracker NIR680 and plated on black glass-bottom 24-well plates
285 (Sensoplate, Greiner Bio-One). Cells were transfected with saRNA or treated with 0.5 μM
286 staurosporine (Cayman Chemical) as a positive control.

287 Annexin V-CF800 conjugate (Biotium) was diluted to 250 ng/ml in Live Cell Imaging Solution
288 (Invitrogen). On each day of the assay, wells were washed with Live Cell Imaging Solution and
289 replaced with diluted Annexin V-CF800 solution. Plates were incubated at 37°C for 15 minutes.
290 Following incubation, plates were washed 3 times with Live Cell Imaging Solution before imaging
291 the 700 and 800 channels with an Odyssey M imager set to +1.45 mm image offset and 100 μm
292 resolution.

293 Image analysis was performed using ImageJ. To correct for unidirectional spectral bleed-through of
294 BioTracker NIR680 into the 800-channel, subtractive compensation was applied by dividing the
295 700-channel image by a factor of 800 and then subtracting it from the 800-channel image. Due to
296 the presence of a small number of high-intensity speckles in the 800-channel image, area rather
297 than fluorescence intensity was quantified. The display range of the 800-channel image was set
298 between 0.25 and 2.5 and the image was thresholded using the method of Li[47]. The area of
299 thresholded pixels within each well was then quantified and adjusted based on the BioTracker
300 signal before transfection to account for variations in cell numbers. Data was then normalized to
301 the average of the mock transfection condition.

302

303 *Calcein AM staining*

304 Calcein AM (Invitrogen) staining was performed according to the manufacturer's protocol. Briefly,
305 cells were washed with HBSS and incubated with 2 μM Calcein AM (diluted in HBSS) at 37°C for 30
306 minutes. Following three washes, cells were imaged in Live Cell Imaging Solution, and the 488-
307 channel image was captured using an Odyssey M imager.

308 Although Calcein AM and EGFP share overlapping spectra, Calcein AM fluorescence was typically
309 much higher than EGFP, making EGFP's contribution to the measured Calcein AM signal negligible
310 in most cases. However, when the E3 construct was used, EGFP expression was sufficient to
311 interfere with the signal. To address this, in experiments that included use of the E3 construct, a
312 488-channel image was captured prior to Calcein AM application and subtracted from the post-
313 application image to accurately measure Calcein AM fluorescence.

314 Fluorescence intensity was quantified using ImageJ. In experiments where BioTracker was used,
315 fluorescence values were corrected by the pre-transfection BioTracker signal to account for
316 differences in starting cell numbers.

317

318 *In-cell western assay*

319 Cells were plated on black, glass-bottom 24-well plates. Alongside mock and saRNA transfections,
320 one well was reserved for background subtraction, which received no treatment. Cells were fixed
321 with 4% paraformaldehyde for 10 minutes at room temperature, followed by two washes with tris-
322 buffered saline (TBS). Permeabilization was then performed using 0.1% Triton X-100 in TBS for 10
323 minutes, followed by two additional TBS washes. After permeabilization, cells were blocked with
324 Intercept TBS Blocking Buffer (LI-COR) for 1 hour at room temperature with gentle agitation.

325 Primary antibodies were diluted in Intercept Blocking Buffer and incubated with the cells overnight
326 at 4°C. The background subtraction well was incubated with blocking buffer alone, without primary
327 antibodies. The following primary antibodies were used: Phospho-eIF2α (Ser51) (D9G8) XP rabbit
328 monoclonal (1:200, #3398, Cell Signaling Technology), eIF2α (L57A5) mouse monoclonal (1:200,
329 #2103, Cell Signaling Technology), PKR rabbit polyclonal (1:500, #18244-1-AP, Proteintech),
330 Phospho-eIF4E (S209) rabbit monoclonal (1:200, #ab76256, Abcam), eIF4E mouse monoclonal
331 (5D11) (1:200, #MA1-089, Invitrogen), and fibroblast activation protein (73.3) mouse monoclonal
332 (20 µg/ml, #BE0374, InVivoMAb). Except for the fibroblast activation protein antibody, which was
333 conjugated to DyLight 800 using the manufacturer's DyLight Antibody Labeling Kit (#53062, Thermo
334 Scientific), all primary antibodies were unconjugated.

335 After washing the wells three times with TBS, cells were incubated for 1 hour at room temperature
336 with the appropriate secondary antibodies or normalization stain, with gentle agitation. The
337 secondary antibodies used were goat anti-mouse IRDye 800CW (1:800), donkey anti-rabbit IRDye
338 800CW (1:800), donkey anti-mouse IRDye 680RD (1:800), and CellTag 700 (1:500), all from LI-COR.
339 The background subtraction well received secondary antibody but no CellTag. Following four
340 additional washes with TBS, the plate was inverted and gently tapped on absorbent paper to
341 remove excess liquid. The plate was then imaged using the Odyssey M imager with LI-COR
342 Acquisition software using a plate offset of +1.45 and 100 µm resolution. Signal quantification was
343 carried out using Empiria Studio software (LI-COR).

344

345 *RNA integrity analysis*

346 FLS were plated in 6-well plates and transfected with either saRNA or subjected to mock
347 transfection. After 26-30 hours, cells were harvested by scraping in 350 µl RLT buffer (QIAGEN)
348 supplemented with 10 µl/ml β-mercaptoethanol (Sigma). Cell lysates were homogenized using
349 QIAshredder columns (QIAGEN), and total RNA was extracted using the RNeasy Mini Kit (QIAGEN)
350 according to the manufacturer's instructions. RNA quantity and quality were initially assessed using
351 a N60 nanophotometer (Implen). Samples were aliquoted and stored at -80°C until further analysis.
352 For detailed quality assessment, samples were transported on dry ice and analyzed using the RNA
353 Pico Kit on the 2100 Bioanalyzer system (Agilent), performed by Cambridge Genomic Services. RNA

Integrity Number (RIN) values were determined for each sample, and the differences in RIN between saRNA-transfected and mock-transfected conditions were calculated.

Bead-based immunoassay

FLS were stained with BioTracker and seeded onto 6-well plates. After transfection, the saRNA-lipofectamine complexes were replaced with 2 ml of fresh FLS media. Two days later, supernatants were collected and stored at -80°C until analysis. On the day of analysis, the supernatant was thawed on ice, and levels of 13 innate immune-related cytokines (IFN-γ, CXCL1, TNF-α, MCP-1, IL-12p70, CCL5, IL-1β, CXCL10, GM-CSF, IL-10, IFN-β, IFN-α, and IL-6) were measured using the LEGENDplex Mouse Anti-Virus Response Panel (740621, BioLegend) following the manufacturer's protocol. Samples were run in duplicate. A custom 3D-printed PETG vacuum manifold (designed with Fusion 360) was used for vacuum filtration, and beads were analyzed using a CytoPLEX LX flow cytometer (Beckman Coulter). Data analysis was performed with the LEGENDplex Qognit Data Analysis Suite (BioLegend). To account for differences in cell numbers between wells, cytokine levels were corrected based on the BioTracker signal before transfection.

ML336 experiments

ML336 (Cayman Chemical) was dissolved in DMSO (Sigma) at a stock concentration of 10 mM, and aliquots were stored at -20°C. For treatments, ML336 was added to cell cultures at a final concentration of 1 μM, while vehicle control cultures received 0.01% DMSO.

Statistical analysis

All statistical analyses were conducted using GraphPad Prism 9, with specific tests detailed in the corresponding figure legends. All statistical tests were two-sided tests.

Data Availability

The data that support the findings of this study are available on the Figshare repository at 10.6084/m9.figshare.27091972. There are no restrictions on data availability.

The 3D printed vacuum manifold compatible with the LEGENDplex assay has been deposited in the NIH 3D print exchange (3DPX-021388).

Code Availability

The code for the unmixing analysis is available at https://github.com/lariferg/spectral_unmixing.

388 **References**

389 1. Silva-Pilipich, N., Beloki, U., Salaberry, L. & Smerdou, C. Self-Amplifying RNA: A Second
390 Revolution of mRNA Vaccines against COVID-19. *Vaccines (Basel)* **12**, 318 (2024).
391 2. Bloom, K., van den Berg, F. & Arbuthnot, P. Self-amplifying RNA vaccines for infectious
392 diseases. *Gene Ther* **28**, 117–129 (2021).
393 3. Pietilä, M. K., Hellström, K. & Ahola, T. Alphavirus polymerase and RNA replication. *Virus*
394 *Research* **234**, 44–57 (2017).
395 4. Maruggi, G., Zhang, C., Li, J., Ulmer, J. B. & Yu, D. mRNA as a Transformative Technology for
396 Vaccine Development to Control Infectious Diseases. *Mol Ther* **27**, 757–772 (2019).
397 5. Gorchakov, R., Frolova, E., Williams, B. R. G., Rice, C. M. & Frolov, I. PKR-Dependent and -
398 Independent Mechanisms Are Involved in Translational Shutoff during Sindbis Virus Infection.
399 *Journal of Virology* **78**, 8455–8467 (2004).
400 6. Terenzi, F. *et al.* The antiviral enzymes PKR and RNase L suppress gene expression from viral
401 and non-viral based vectors. *Nucleic Acids Res* **27**, 4369–4375 (1999).
402 7. Urban, C. *et al.* Apoptosis induced by Semliki Forest virus is RNA replication dependent and
403 mediated via Bak. *Cell Death Differ* **15**, 1396–1407 (2008).
404 8. Pepini, T. *et al.* Induction of an IFN-Mediated Antiviral Response by a Self-Amplifying RNA
405 Vaccine: Implications for Vaccine Design. *The Journal of Immunology* **198**, 4012–4024 (2017).
406 9. Blakney, A. K., Ip, S. & Geall, A. J. An Update on Self-Amplifying mRNA Vaccine Development.
407 *Vaccines (Basel)* **9**, 97 (2021).
408 10. Minnaert, A.-K. *et al.* Strategies for controlling the innate immune activity of conventional and
409 self-amplifying mRNA therapeutics: Getting the message across. *Adv Drug Deliv Rev* **176**,
410 113900 (2021).
411 11. Blakney, A. K. *et al.* Innate Inhibiting Proteins Enhance Expression and Immunogenicity of Self-
412 Amplifying RNA. *Mol Ther* **29**, 1174–1185 (2021).
413 12. Beissert, T. *et al.* Improvement of In Vivo Expression of Genes Delivered by Self-Amplifying RNA
414 Using Vaccinia Virus Immune Evasion Proteins. *Hum Gene Ther* **28**, 1138–1146 (2017).
415 13. Yoshioka, N. *et al.* Efficient Generation of Human iPS Cells by a Synthetic Self-Replicative RNA.
416 *Cell Stem Cell* **13**, 10.1016/j.stem.2013.06.001 (2013).
417 14. Szczerba, M. *et al.* Small Hero with Great Powers: Vaccinia Virus E3 Protein and Evasion of the
418 Type I IFN Response. *Biomedicines* **10**, 235 (2022).
419 15. Kalveram, B. & Ikegami, T. Toscana Virus NSs Protein Promotes Degradation of Double-
420 Stranded RNA-Dependent Protein Kinase. *J Virol* **87**, 3710–3718 (2013).
421 16. Drappier, M. *et al.* A novel mechanism of RNase L inhibition: Theiler's virus L* protein prevents
422 2-5A from binding to RNase L. *PLoS Pathog* **14**, e1006989 (2018).
423 17. Maglaviceanu, A., Wu, B. & Kapoor, M. Fibroblast-like synoviocytes: Role in synovial fibrosis
424 associated with osteoarthritis. *Wound Repair and Regeneration* **29**, 642–649 (2021).
425 18. Mousavi, M. J. *et al.* Transformation of fibroblast-like synoviocytes in rheumatoid arthritis; from
426 a friend to foe. *Autoimmun Highlights* **12**, 3 (2021).
427 19. Santoro, M. G., Rossi, A. & Amici, C. NF-κB and virus infection: who controls whom. *The EMBO*
428 *Journal* **22**, 2552–2560 (2003).

429 20. Mitchell, J. P. & Carmody, R. J. Chapter Two - NF-κB and the Transcriptional Control of
430 Inflammation. in *International Review of Cell and Molecular Biology* (ed. Loos, F.) vol. 335 41–
431 84 (Academic Press, 2018).
432 21. Lee, Y.-R. *et al.* Inhibition of IL-1β-mediated inflammatory responses by the IκBα super-
433 repressor in human fibroblast-like synoviocytes. *Biochemical and Biophysical Research*
434 *Communications* **378**, 90–94 (2009).
435 22. Brown, K., Gerstberger, S., Carlson, L., Franzoso, G. & Siebenlist, U. Control of IκB-α Proteolysis
436 by Site-Specific, Signal-Induced Phosphorylation. *Science* **267**, 1485–1488 (1995).
437 23. Yan, X., Liu, Z. & Chen, Y. Regulation of TGF-β signaling by Smad7. *Acta Biochimica et*
438 *Biophysica Sinica* **41**, 263–272 (2009).
439 24. Sobah, M. L., Liongue, C. & Ward, A. C. SOCS Proteins in Immunity, Inflammatory Diseases,
440 and Immune-Related Cancer. *Front Med (Lausanne)* **8**, 727987 (2021).
441 25. Dimitriou, I. D. *et al.* Putting out the fire: coordinated suppression of the innate and adaptive
442 immune systems by SOCS1 and SOCS3 proteins. *Immunological Reviews* **224**, 265–283
443 (2008).
444 26. Boyd, D. F. *et al.* Exuberant fibroblast activity compromises lung function via ADAMTS-4. *Nature*
445 **587**, 466–471 (2020).
446 27. Krausgruber, T. *et al.* Structural cells are key regulators of organ-specific immune response.
447 *Nature* **583**, 296–302 (2020).
448 28. Croft, A. P. *et al.* Distinct fibroblast subsets drive inflammation and damage in arthritis. *Nature*
449 **570**, 246–251 (2019).
450 29. Bauer, S. *et al.* Fibroblast activation protein is expressed by rheumatoid myofibroblast-like
451 synoviocytes. *Arthritis Res Ther* **8**, R171 (2006).
452 30. Zhang, H. E. *et al.* Identification of Novel Natural Substrates of Fibroblast Activation Protein-
453 alpha by Differential Degradomics and Proteomics. *Mol Cell Proteomics* **18**, 65–85 (2019).
454 31. Wäldele, S. *et al.* Deficiency of fibroblast activation protein alpha ameliorates cartilage
455 destruction in inflammatory destructive arthritis. *Arthritis Res Ther* **17**, 12 (2015).
456 32. Chung, D. *et al.* ML336: Development of Quinazolinone-Based Inhibitors Against Venezuelan
457 Equine Encephalitis Virus (VEEV). in *Probe Reports from the NIH Molecular Libraries Program*
458 (National Center for Biotechnology Information (US), Bethesda (MD), 2010).
459 33. Iimuro, Y. *et al.* NFkappaB prevents apoptosis and liver dysfunction during liver regeneration. *J*
460 *Clin Invest* **101**, 802–811 (1998).
461 34. Karin, M. & Lin, A. NF-κB at the crossroads of life and death. *Nat Immunol* **3**, 221–227 (2002).
462 35. Stolfi, C. *et al.* A functional role for Smad7 in sustaining colon cancer cell growth and survival.
463 *Cell Death Dis* **5**, e1073–e1073 (2014).
464 36. Halder, S. K., Beauchamp, R. D. & Datta, P. K. Smad7 induces tumorigenicity by blocking TGF-
465 β-induced growth inhibition and apoptosis. *Experimental Cell Research* **307**, 231–246 (2005).
466 37. Kimura, A., Naka, T., Nagata, S., Kawase, I. & Kishimoto, T. SOCS-1 suppresses TNF-α-induced
467 apoptosis through the regulation of Jak activation. *International Immunology* **16**, 991–999
468 (2004).
469 38. Zitzmann, K. *et al.* SOCS1 Silencing Enhances Antitumor Activity of Type I IFNs by Regulating
470 Apoptosis in Neuroendocrine Tumor Cells. *Cancer Research* **67**, 5025–5032 (2007).

39. Hariri, F. *et al*. The eukaryotic translation initiation factor eIF4E is a direct transcriptional target of NF-κB and is aberrantly regulated in acute myeloid leukemia. *Leukemia* **27**, 2047–2055 (2013).
40. Uttam, S., Wong, C., Price, T. J. & Khoutorsky, A. eIF4E-Dependent Translational Control: A Central Mechanism for Regulation of Pain Plasticity. *Front Genet* **9**, 470 (2018).
41. Siddiqui, N. & Sonenberg, N. Signalling to eIF4E in cancer. *Biochemical Society Transactions* **43**, 763–772 (2015).
42. Gkogkas, C. G. *et al*. Autism-related deficits via dysregulated eIF4E-dependent translational control. *Nature* **493**, 371–377 (2013).
43. Syntichaki, P., Troulinaki, K. & Tavernarakis, N. eIF4E function in somatic cells modulates ageing in Caenorhabditis elegans. *Nature* **445**, 922–926 (2007).
44. Gadella, T. W. J. *et al*. mScarlet3: a brilliant and fast-maturing red fluorescent protein. *Nat Methods* **20**, 541–545 (2023).
45. Costantini, L. M. *et al*. A palette of fluorescent proteins optimized for diverse cellular environments. *Nat Commun* **6**, 7670 (2015).
46. Chakrabarti, S. *et al*. Sensitization of knee-innervating sensory neurons by tumor necrosis factor-α-activated fibroblast-like synoviocytes: an in vitro, coculture model of inflammatory pain. *Pain* **161**, 2129–2141 (2020).
47. Li, C. H. & Lee, C. K. Minimum cross entropy thresholding. *Pattern Recognition* **26**, 617–625 (1993).

Acknowledgements

The authors gratefully acknowledge the Cambridge Advanced Imaging Centre, the flow cytometry facility from the School of the Biological Sciences, and Cambridge Genomic Services for their support & assistance in this work. The authors would like to thank Dr. Paul Miller for providing the pDx_mScarlet3 plasmid and Dr. Alex Cloake for providing the pIRES2-EGFP plasmid used in this study. T.K.L. acknowledges support from a UKRI guarantee Marie Skłodowska-Curie Postdoctoral Fellowship [EP/X023117/1]. A.R. and L.W.P. disclose support from AstraZeneca PhD studentships [G115018 and G113502, respectively]. L.F. discloses support from funding provided by the MRC Postdoctoral Training Scheme. E.St.J.S. acknowledges funding from the UKRI and Versus Arthritis [MR/W002426/1] as part of the ADVANTAGE visceral pain consortium through the Advanced Pain Discovery Platform (APDP) and the Wellcome Trust [225856/Z/22/Z].

Author Information

Department of Pharmacology, University of Cambridge, Cambridge, UK
Tony K.Y. Lim, Anne Ritoux, Luke W. Paine, Ewan St. John Smith

MRC Laboratory of Molecular Biology, Cambridge, UK
Larissa Ferguson

Correspondence can be addressed to Tony K.Y. Lim or Ewan St. John Smith.

Competing interests

The authors declare no competing interests.

Contributions

Tony K.Y. Lim: Conceptualization, Formal analysis, Funding acquisition, Investigation, Methodology, Resources, Supervision, Visualisation, Writing – Original draft

Anne Ritoux: Investigation

Luke W. Paine: Investigation

Larissa Ferguson: Software

Tawab Abdul: Methodology

Ewan St. John Smith: Conceptualization, Formal analysis, Funding acquisition, Resources, Supervision, Visualisation, Writing – reviewing and editing

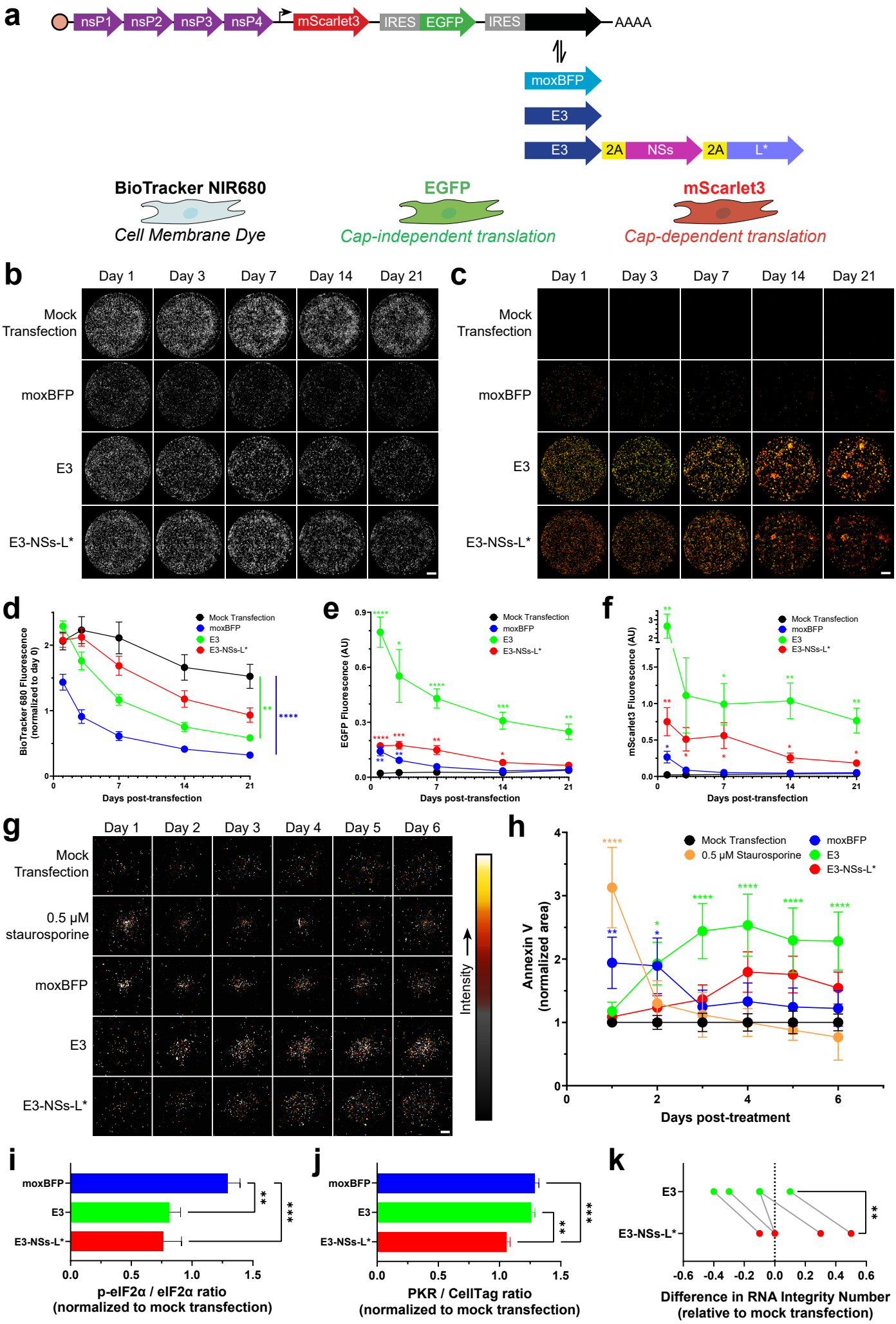
a
nsP1
nsP2
nsP3
nsP4
mScarlet3
IRES
EGFP
IRES
AAAA
moxBFP
E3
E3
2A
NSs
2A
L*
BioTracker NIR680
Cell Membrane Dye
EGFP
Cap-independent translation
mScarlet3
Cap-dependent translation
b
Day 1
Day 3
Day 7
Day 14
Day 21
Mock Transfection
moxBFP
E3
E3-NSs-L*
c
Day 1
Day 3
Day 7
Day 14
Day 21
Mock Transfection
moxBFP
E3
E3-NSs-L*
d
BioTracker 680 Fluorescence (normalized to day 0)
Days post-transfection
Mock Transfection
moxBFP
E3
E3-NSs-L*
e
EGFP Fluorescence (AU)
Days post-transfection
Mock Transfection
moxBFP
E3
E3-NSs-L*
f
mScarlet3 Fluorescence (AU)
Days post-transfection
Mock Transfection
moxBFP
E3
E3-NSs-L*
g
Day 1
Day 2
Day 3
Day 4
Day 5
Day 6
Mock Transfection
0.5 μM staurosporine
moxBFP
E3
E3-NSs-L*
Intensity
h
Annexin V (normalized area)
Days post-treatment
Mock Transfection
0.5 μM Staurosporine
moxBFP
E3
E3-NSs-L*
i
moxBFP
E3
E3-NSs-L*
p-eIF2α / eIF2α ratio
(normalized to mock transfection)
j
moxBFP
E3
E3-NSs-L*
PKR / CellTag ratio
(normalized to mock transfection)
k
E3
E3-NSs-L*
Difference in RNA Integrity Number
(relative to mock transfection)

524 **Figure 1. Multi-target cap-independent co-expression of viral immune evasion proteins**
525 **reduces cytotoxicity of saRNA.**

526 **a**, Schematic illustrating the different saRNA constructs tested and the *in vitro* reporter assay using
527 primary mouse FLS. The angled arrow signifies the subgenomic promoter.
528 **b**, Representative images of BioTracker staining over 3 weeks in FLS transfected with different
529 saRNA constructs. Scale bar = 5 mm.
530 **c**, Representative images of EGFP (green) and mScarlet3 (red) expression over 3 weeks in FLS
531 transfected with different saRNA constructs. Scale bar = 5 mm.
532 **d**, Quantification of BioTracker fluorescence intensity (n = 11). Statistical significance of main
533 treatment effects compared to mock transfection was determined by two-way RM ANOVA with
534 Dunnett's multiple comparisons test.
535 **e**, Quantification of EGFP fluorescence intensity (n = 11). Statistical significance of treatment
536 effects at each time point compared to mock transfection was determined by two-way RM ANOVA
537 with Greenhouse–Geisser correction and Dunnett's multiple comparisons test.
538 **f**, Quantification of mScarlet3 fluorescence intensity (n = 11). Statistical significance of treatment
539 effects at each time point compared to mock transfection was determined by two-way RM ANOVA
540 with Greenhouse–Geisser correction and Dunnett's multiple comparisons test.
541 **g**, Representative cropped images of Annexin V-CF800 staining over time in FLS transfected with
542 different saRNA constructs. Scale bar = 1.5 mm.
543 **h**, Annexin V signal is presented as the area of positive pixels determined by Li thresholding
544 normalized to the average of the mock transfection group (n = 6). Statistical significance of
545 treatment effects at each time point compared to mock transfection was determined by two-way
546 RM ANOVA and Bonferonni's multiple comparisons test using one family for all comparisons.
547 **i**, In-cell western analysis of phosphorylated eIF2α levels after 2 days of transfection with different
548 saRNA constructs presented as fold-change over mock transfected cells (n = 5). Statistical
549 significance was determined by one-way RM ANOVA and Tukey's multiple comparisons test.
550 **j**, In-cell western analysis of PKR levels after 2 days of transfection with different saRNA constructs
551 presented as fold-change over mock transfected cells (n = 4). Statistical significance was
552 determined by one-way RM ANOVA and Tukey's multiple comparisons test.
553 **k**, RNA integrity analysis after 1 day of transfection with different saRNA constructs presented as
554 the difference in RNA Integrity Number relative to mock transfected cells (n = 5). Statistical
555 significance was determined by paired t test.
556 For all statistical reporting, *P < 0.05, **P < 0.01, ***P < 0.001 and ****P < 0.0001. Data are
557 presented as mean ± SEM.
558 nsP, Venezuelan equine encephalitis virus non-structural protein; IRES, encephalomyocarditis virus
559 internal ribosome entry site; moxBFP, monomeric oxidizing environment-optimized blue
560 fluorescent protein; E3, Vaccinia virus E3 protein; NSs, Toscana Virus non-structural NSs protein;
561 L*, Theiler's murine encephalomyelitis virus L* protein; 2A, self-cleaving 2A peptide.

562

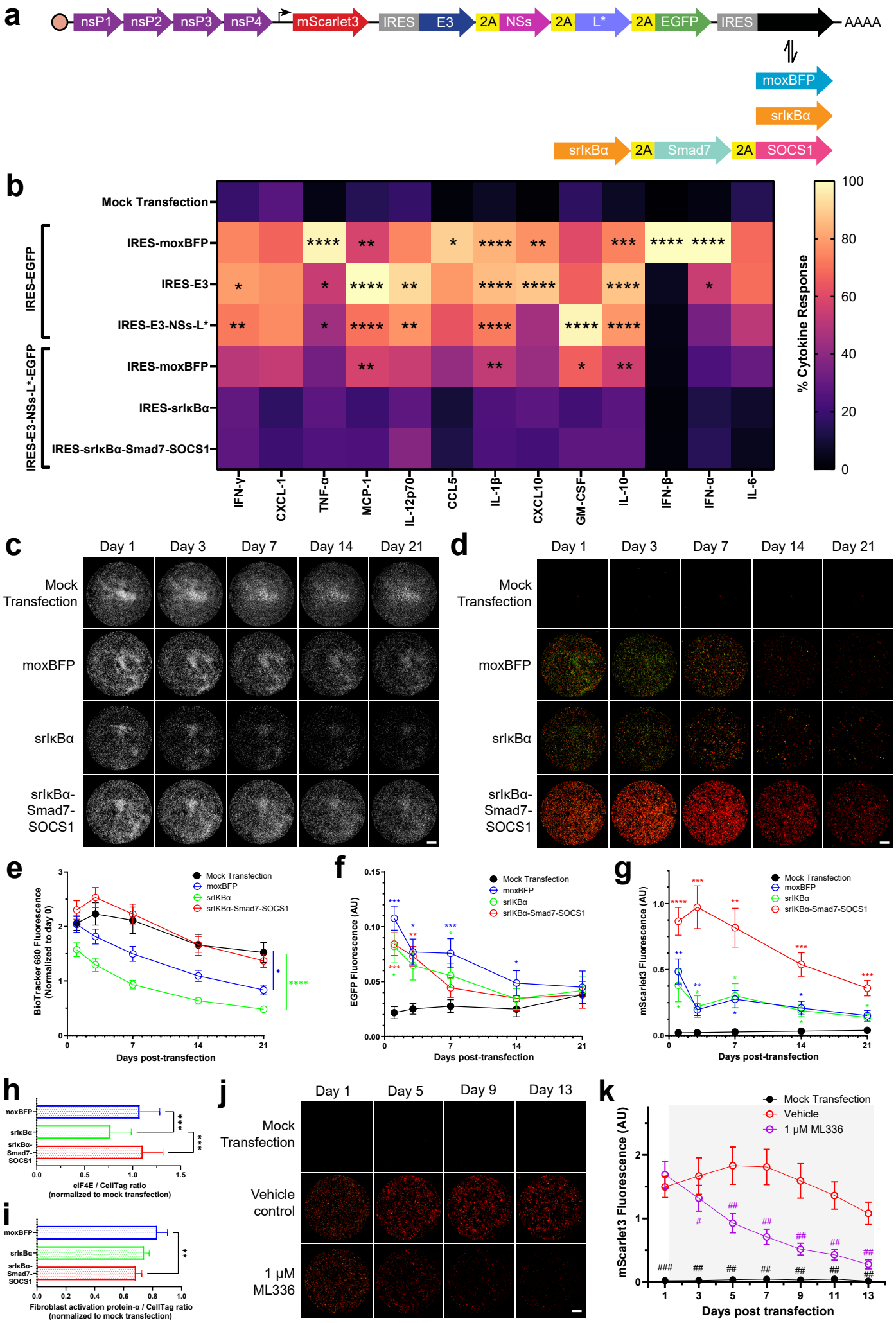
a
nsP1
nsP2
nsP3
nsP4
mScarlet3
IRES
E3
2A
NSs
2A
L*
2A
EGFP
IRES
AAAA
moxBFP
srIκBα
srIκBα
2A
Smad7
2A
SOCS1
b
Mock Transfection
IRES-EGFP
IRES-moxBFP
IRES-E3
IRES-E3-NSs-L*
IRES-E3-NSs-L*-EGFP
IRES-moxBFP
IRES-srIκBα
IRES-srIκBα-Smad7-SOCS1
IFN-γ
CXCL-1
TNF-α
MCP-1
IL-12p70
CCL5
IL-1β
CXCL10
GM-CSF
IL-10
IFN-β
IFN-α
IL-6
% Cytokine Response
100
80
60
40
20
0
c
Day 1
Day 3
Day 7
Day 14
Day 21
Mock Transfection
moxBFP
srIκBα
srIκBα-Smad7-SOCS1
d
Day 1
Day 3
Day 7
Day 14
Day 21
Mock Transfection
moxBFP
srIκBα
srIκBα-Smad7-SOCS1
e
BioTracker 680 Fluorescence (Normalized to day 0)
Days post-transfection
Mock Transfection
moxBFP
srIKBα
srIKBα-Smad7-SOCS1
f
EGFP Fluorescence (AU)
Days post-transfection
Mock Transfection
moxBFP
srIKBα
srIKBα-Smad7-SOCS1
g
mScarlet3 Fluorescence (AU)
Days post-transfection
Mock Transfection
moxBFP
srIKBα
srIKBα-Smad7-SOCS1
h
noxBFP
srIκBα
srIκBα-Smad7-SOCS1
eIF4E / CellTag ratio (normalized to mock transfection)
i
moxBFP
srIκBα
srIκBα-Smad7-SOCS1
Fibroblast activation protein-α / CellTag ratio (normalized to mock transfection)
j
Day 1
Day 5
Day 9
Day 13
Mock Transfection
Vehicle control
1 μM ML336
k
Mock Transfection
Vehicle
1 μM ML336
mScarlet3 Fluorescence (AU)
Days post transfection

564 **Figure 2. Multi-target cap-independent co-expression of cellular anti-inflammatory proteins**
565 **reduces immunogenicity while enabling prolonged and reversible transgene expression.**

566 **a**, Schematic illustrating the different saRNA constructs tested.
567 **b**, Levels of anti-viral cytokines in FLS supernatant collected 2 days post-transfection (n = 6).
568 Statistical significance for each cytokine was assessed using one-way ANOVA followed by
569 Bonferroni's multiple comparisons test against the mock transfection control, with a subsequent
570 Bonferroni correction applied to P values to account for multiple independent hypothesis testing.
571 For visualization, cytokine levels were scaled within each biological replicate, with the highest value
572 set to 100% and the mean level displayed on the heatmap.
573 **c**, Representative images of BioTracker staining over 3 weeks in FLS transfected with different
574 saRNA constructs. Scale bar = 5 mm.
575 **d**, Representative images of EGFP (green) and mScarlet3 (red) expression over 3 weeks in FLS
576 transfected with different saRNA constructs. Scale bar = 5 mm.
577 **e**, Quantification of BioTracker fluorescence intensity (n = 11). Statistical significance of main
578 treatment effects compared to mock transfection was determined by two-way RM ANOVA with
579 Dunnett's multiple comparisons test.
580 **f**, Quantification of EGFP fluorescence intensity (n = 11). Statistical significance of treatment
581 effects at each time point compared to mock transfection was determined by two-way RM ANOVA
582 with Greenhouse–Geisser correction and Dunnett's multiple comparisons test.
583 **g**, Quantification of mScarlet3 fluorescence intensity (n = 11). Statistical significance of treatment
584 effects at each time point compared to mock transfection was determined by two-way RM ANOVA
585 with Greenhouse–Geisser correction and Dunnett's multiple comparisons test.
586 **h**, In-cell western analysis of eIF4E levels after 2 days of transfection with different saRNA
587 constructs presented as fold-change over mock transfected cells (n = 6). Statistical significance
588 was determined by one-way RM ANOVA and Tukey's multiple comparisons test.
589 **i**, In-cell western analysis of Fibroblast Activation Protein-α levels after 11 days of transfection with
590 different saRNA constructs presented as fold-change over mock transfected cells (n = 8). Statistical
591 significance was determined by one-way RM ANOVA and Tukey's multiple comparisons test.
592 **j**, Representative images of EGFP (green) and mScarlet3 (red) expression over 3 weeks in FLS
593 transfected with the construct encoding srIκBα-smad7-SOCS1. Cultures were treated with vehicle
594 or 1 μM ML336. Scale bar = 5 mm.
595 **k**, Quantification of mScarlet3 fluorescence intensity in FLS cultures transfected with the construct
596 encoding srIκBα-smad7-SOCS1 and treated with 1 μM ML336 or vehicle (n = 6). Shading represents
597 the treatment time course, starting 1 day post-transfection. Statistical significance compared to
598 the vehicle treated condition was determined by two-way RM ANOVA with Greenhouse–Geisser
599 correction and Dunnett's multiple comparisons test. # P<0.05, ##P<0.01, and ###P<0.01.
600 For all statistical reporting, *P < 0.05, **P < 0.01, ***P < 0.001 and ****P < 0.0001. Data are
601 presented as mean ± SEM.
602 srIκBα, super-repressor inhibitor of κBα; smad7, mothers against decapentaplegic homolog 7;
603 SOCS1, suppressor of cytokine signaling 1.

604

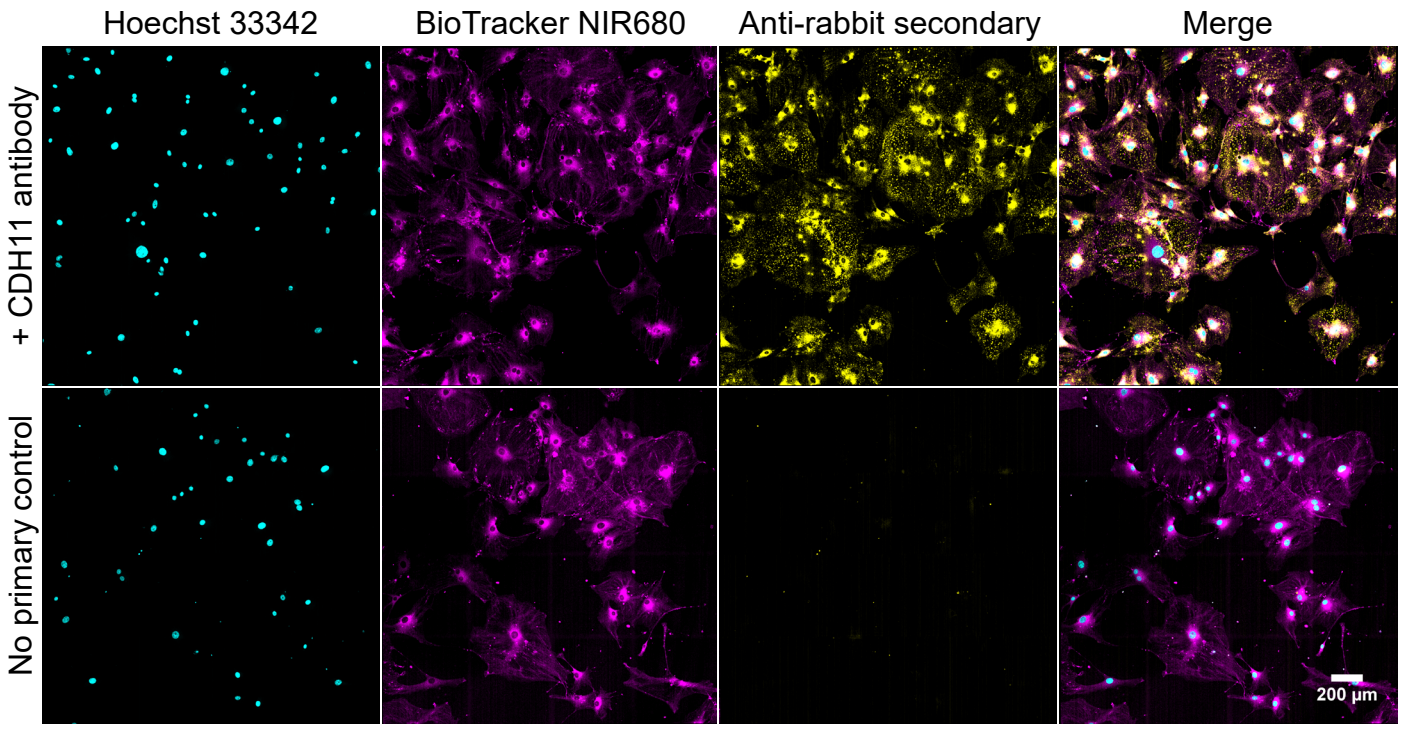

Supplementary Figure 1.

Confocal microscopy images of primary FLS obtained from mouse knees. Cultured cells were immunoreactive for the FLS marker cadherin-11 (CDH11).

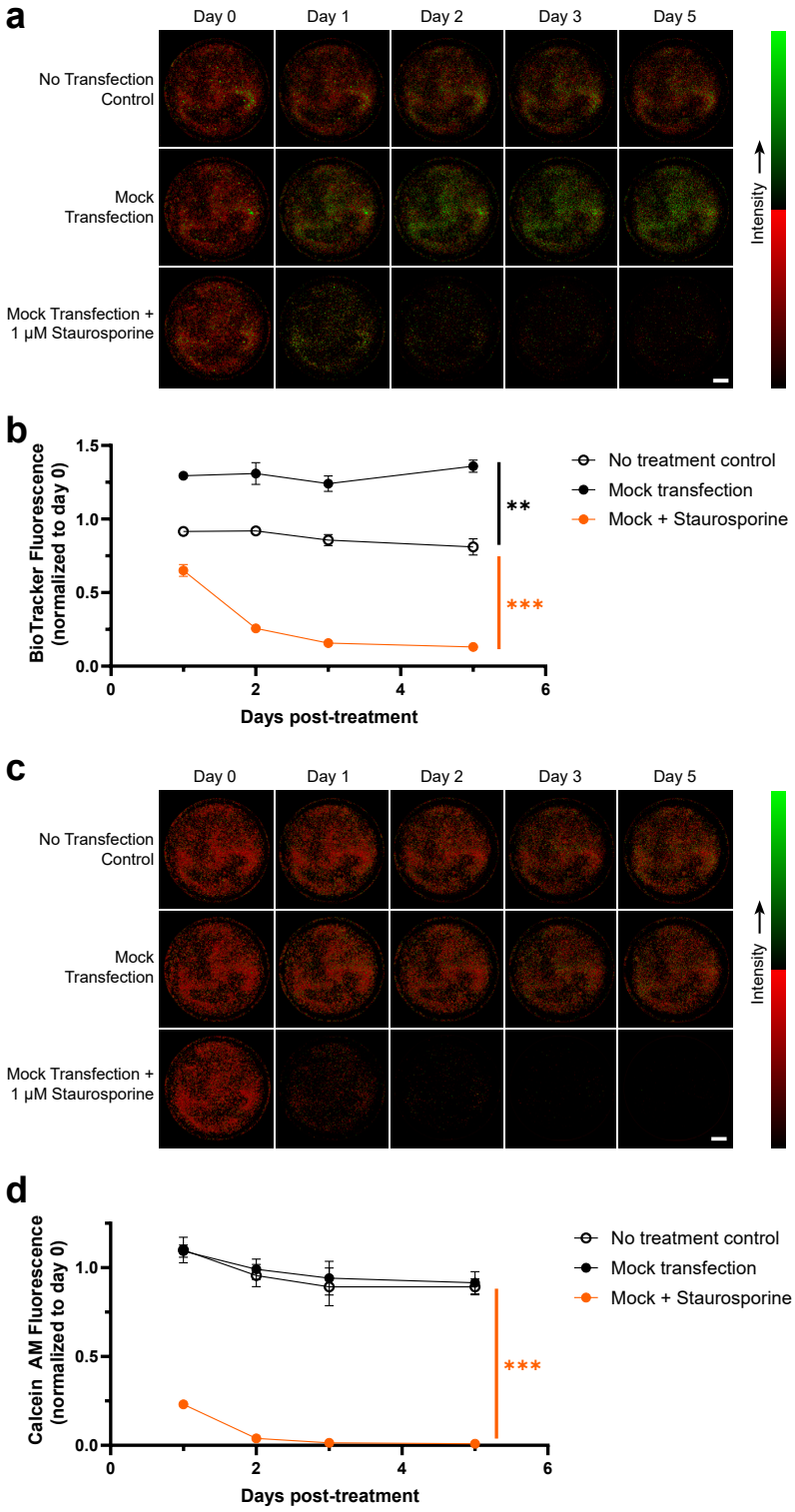

Supplementary Figure 2.

a, Representative images of FLS stained with BioTracker NIR680 after mock transfection and staurosporine treatment. Scale bar = 5 mm.
b, Quantification of BioTracker fluorescence intensity (n = 3). Statistical significance was determined by two-way RM ANOVA with Dunnett's multiple comparisons test comparing groups to the no treatment control.
c, Representative images of FLS stained with calcein AM after mock transfection and staurosporine treatment. Scale bar = 5 mm.
d, Quantification of calcein AM fluorescence intensity (n = 3). Statistical significance was determined by two-way RM ANOVA with Dunnett's multiple comparisons test comparing groups to the no treatment control.
For all statistical reporting, **P < 0.01 and ***P < 0.001. Data are presented as mean ± SEM.

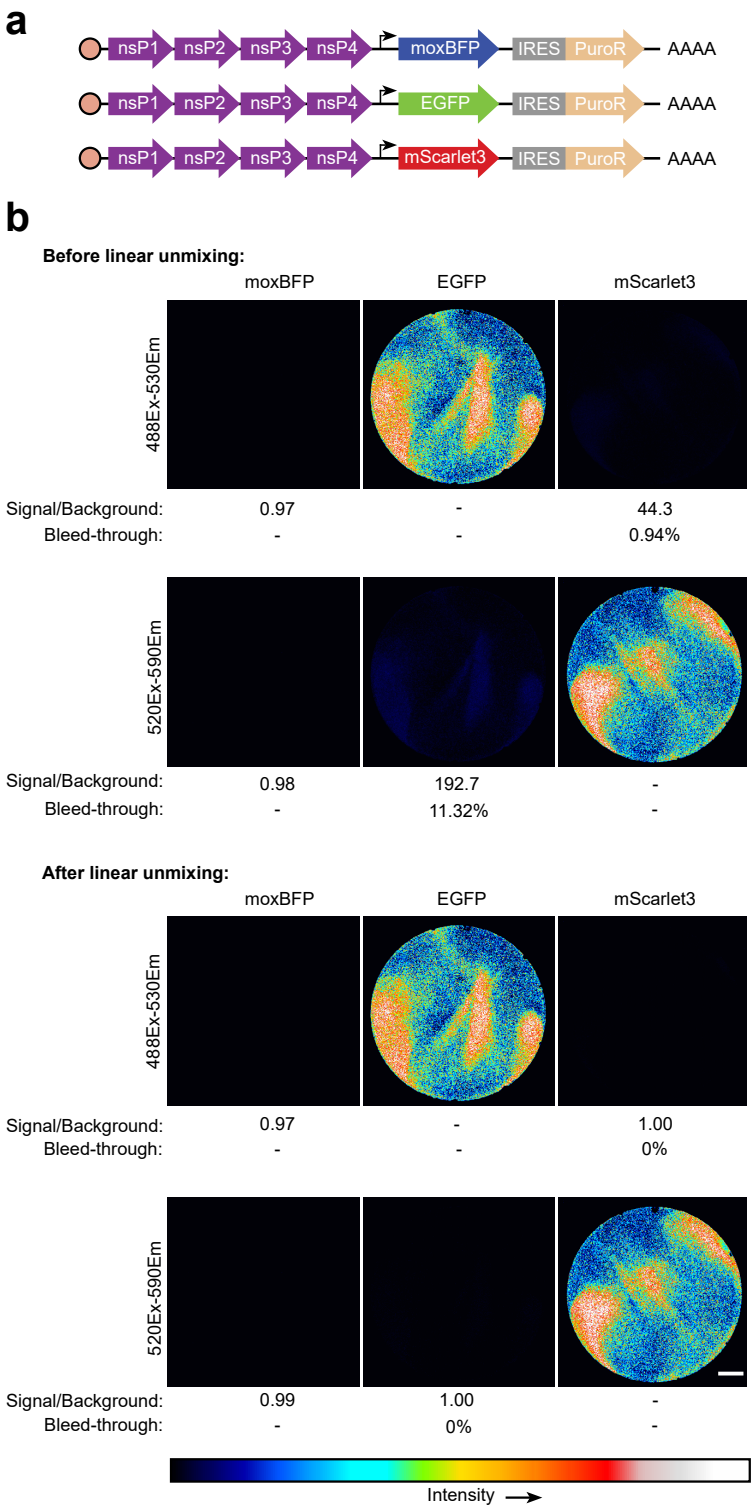

Supplementary Figure 3.

a, Schematic illustrating the different saRNA constructs created for linear unmixing. **b,** tSA201 cells were transfected with the different saRNA constructs. moxBFP was not detectable at the 488Ex-530Em or 520Ex-590Em channels. 11.32% of the EGFP signal bled into the 520Ex-590Em channel, and 0.94% of the mScarlet3 signal bled into the 488Ex-530Em channel. Linear unmixing was used to correct spectral bleed-through between EGFP and mScarlet3. Scale bar = 5 mm.

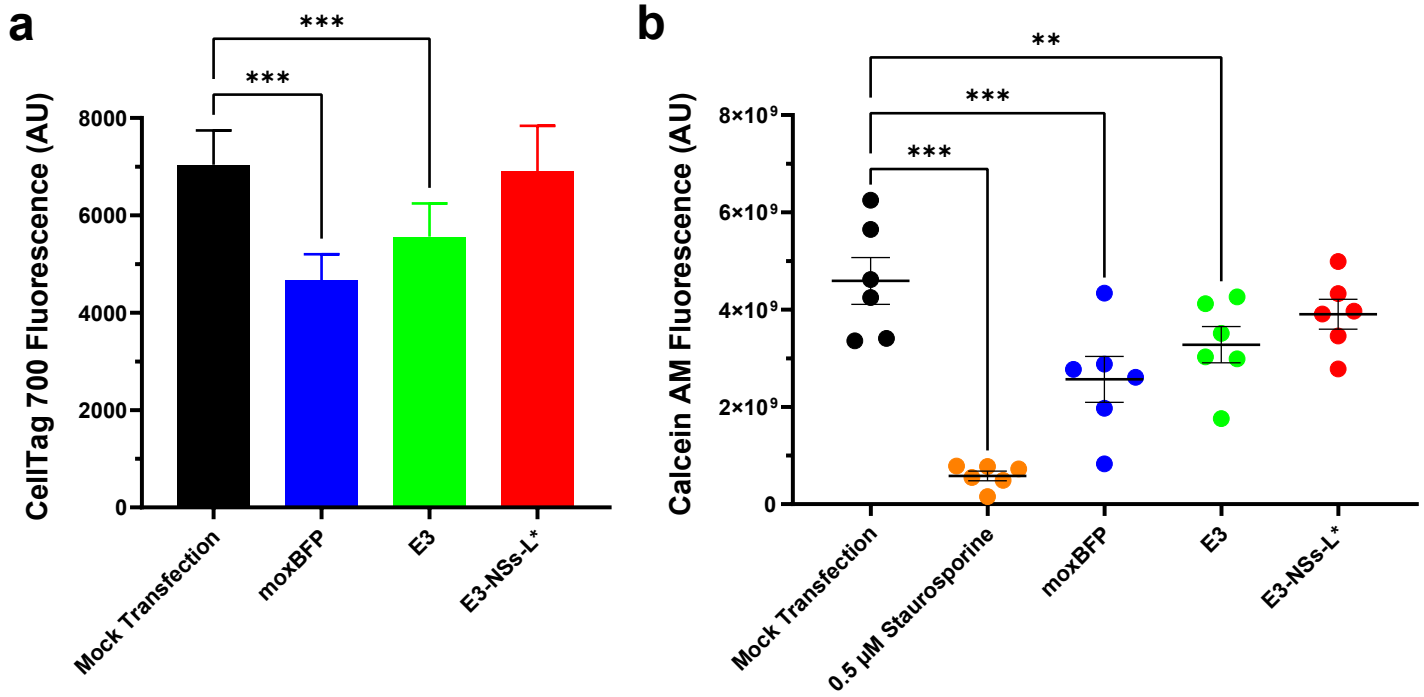

Supplementary Figure 4.

a, Quantification of CellTag staining 2 days post-transfection (n = 24). One sample in the E3 group was identified as an outlier and excluded (ROUT method, Q = 0.1%). Statistical significance was determined by mixed-effects model with matching, Greenhouse–Geisser correction, and Dunnett's multiple comparisons test comparing groups to mock transfection.
b, Quantification of calcein AM staining 7 days post-treatment (n = 6). Statistical significance was determined by one-way RM ANOVA with Greenhouse–Geisser correction and Dunnett's multiple comparisons test comparing groups to mock transfection.
For all statistical reporting, *P < 0.05, **P < 0.01 and ***P < 0.001. Data are presented as mean ± SEM. saRNA constructs used are shown in Figure 1a.

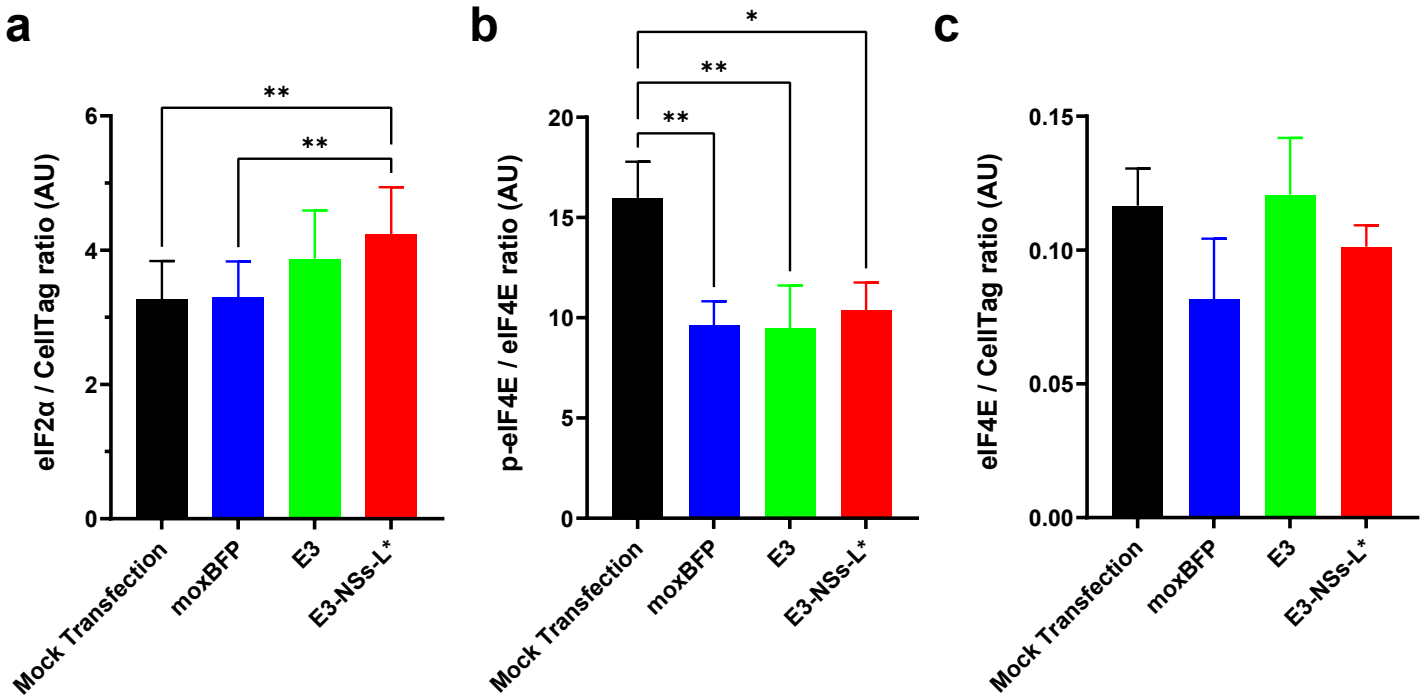

Supplementary Figure 5.

a, In-cell western assay of total eIF2α levels normalized to CellTag (n = 5). Statistical significance was determined by one-way RM ANOVA and Tukey's multiple comparisons test to compare all groups.
b, In-cell western assay of phosphorylated eIF4E levels normalized to total eIF4E levels (n = 6). Statistical significance was determined by one-way RM ANOVA and Tukey's multiple comparisons test to compare all groups.
c, In-cell western assay of total eIF4E levels normalized to CellTag (n = 6). One-way RM ANOVA revealed no significant differences between groups. $F(3,15) = 1.207$, $P=0.3410$.
For all statistical reporting, *$P<0.05$ and **$P < 0.01$. Data are presented as mean ± SEM. saRNA constructs used are shown in Figure 1a.

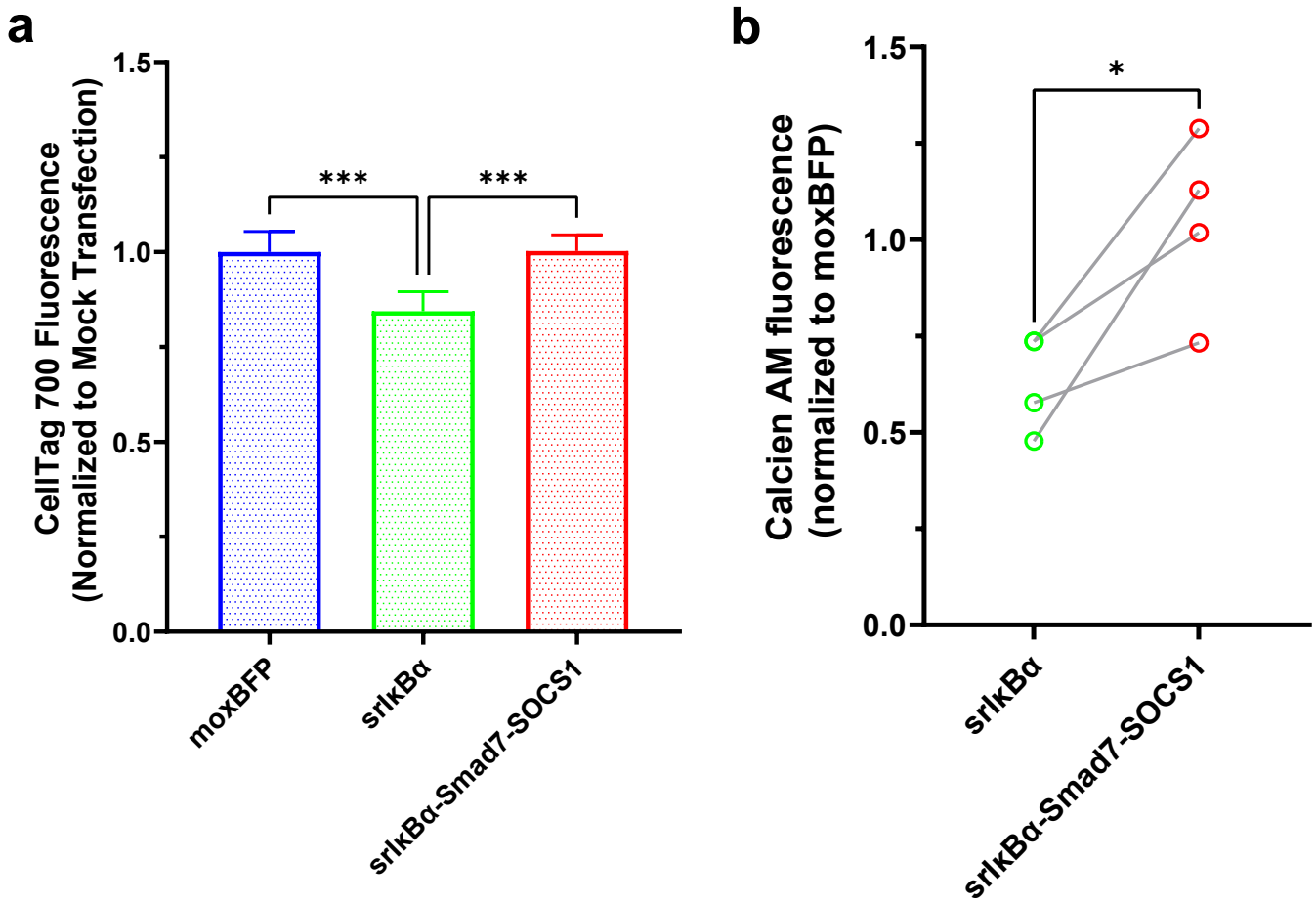

Supplementary Figure 6.

a, Quantification of CellTag staining 2 days post-transfection (n = 20). Data were normalized to mock transfection. Statistical significance was determined by one-way RM ANOVA with Greenhouse–Geisser correction, and Tukey's multiple comparisons test to compare all groups. **b,** Quantification of calcein AM staining 3 days post-treatment (n = 4). Data were normalized to moxBFP transfection. Statistical significance was determined by paired t test. For all statistical reporting, *P<0.05 and ***P < 0.001. Data are presented as mean ± SEM. saRNA constructs used are shown in Figure 2a.

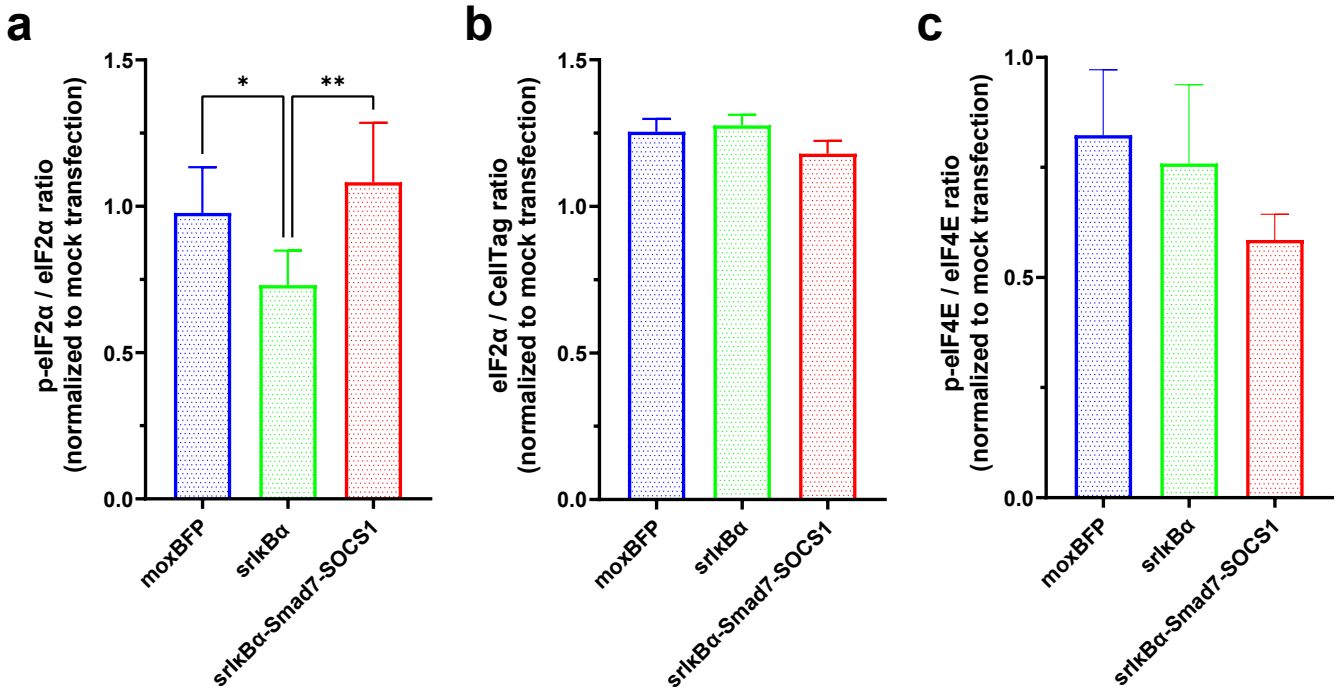

Supplementary Figure 7.

a, In-cell western assay measuring the phosphorylated-eIF2α / total eIF2α ratio (n = 6). Data were normalized to mock transfection. Statistical significance was determined by one-way RM ANOVA and Holm-Šídák's multiple comparisons test to compare all groups.
b, In-cell western assay measuring the total eIF2α / CellTag 700 ratio (n = 6). Data were normalized to mock transfection. One-way RM ANOVA revealed no significant difference between groups. $F(2,8)=3.683$, $P=0.0735$.
c, In-cell western assay measuring phosphorylated-eIF4E / total eIF4E ratio (n = 6). Data were normalized to mock transfection. One-way RM ANOVA revealed no significant difference between groups. $F(2,10)=1.336$, $P=0.3059$.
Data are presented as mean ± SEM. *$P<0.05$ and **$P<0.001$. saRNA constructs used are shown in Figure 2a.

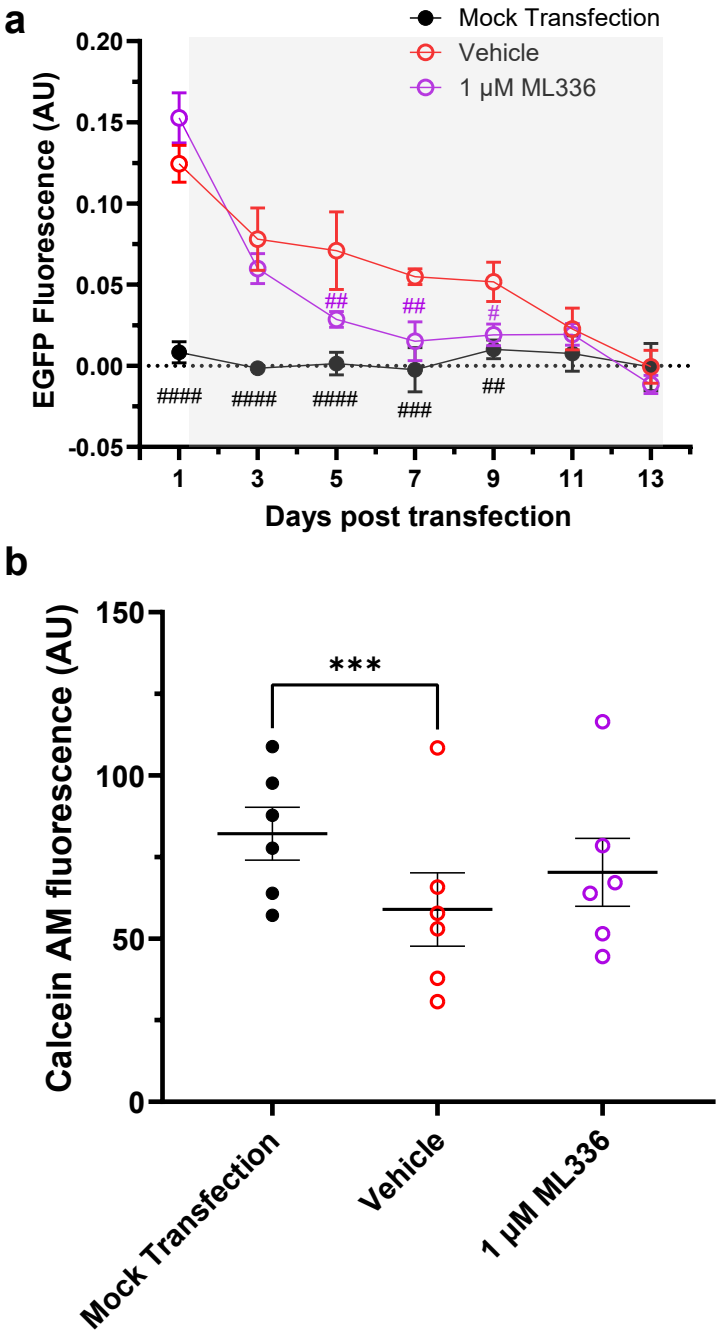

Supplementary Figure 8.

a, Quantification of EGFP fluorescence intensity in FLS cultures transfected with the srIκBα-Smad7-SOCS1 saRNA construct and treated with 1 μM ML336 or vehicle (n = 6). Shading represents the treatment time course, starting 1 day post-transfection. Statistical significance was determined by two-way RM ANOVA and Dunnett's multiple comparisons test to compare groups to vehicle control. #P<0.05, ##P<0.01, ###P<0.001 and ####P<0.0001.

b, Quantification of calcein AM staining after 12 days of vehicle or ML336 treatment (day 13 post-transfection, n = 6). Statistical significance was determined by one-way RM ANOVA and Bonferroni's multiple comparison's test to compare all groups. ***P<0.0001.

Data are presented as mean ± SEM.

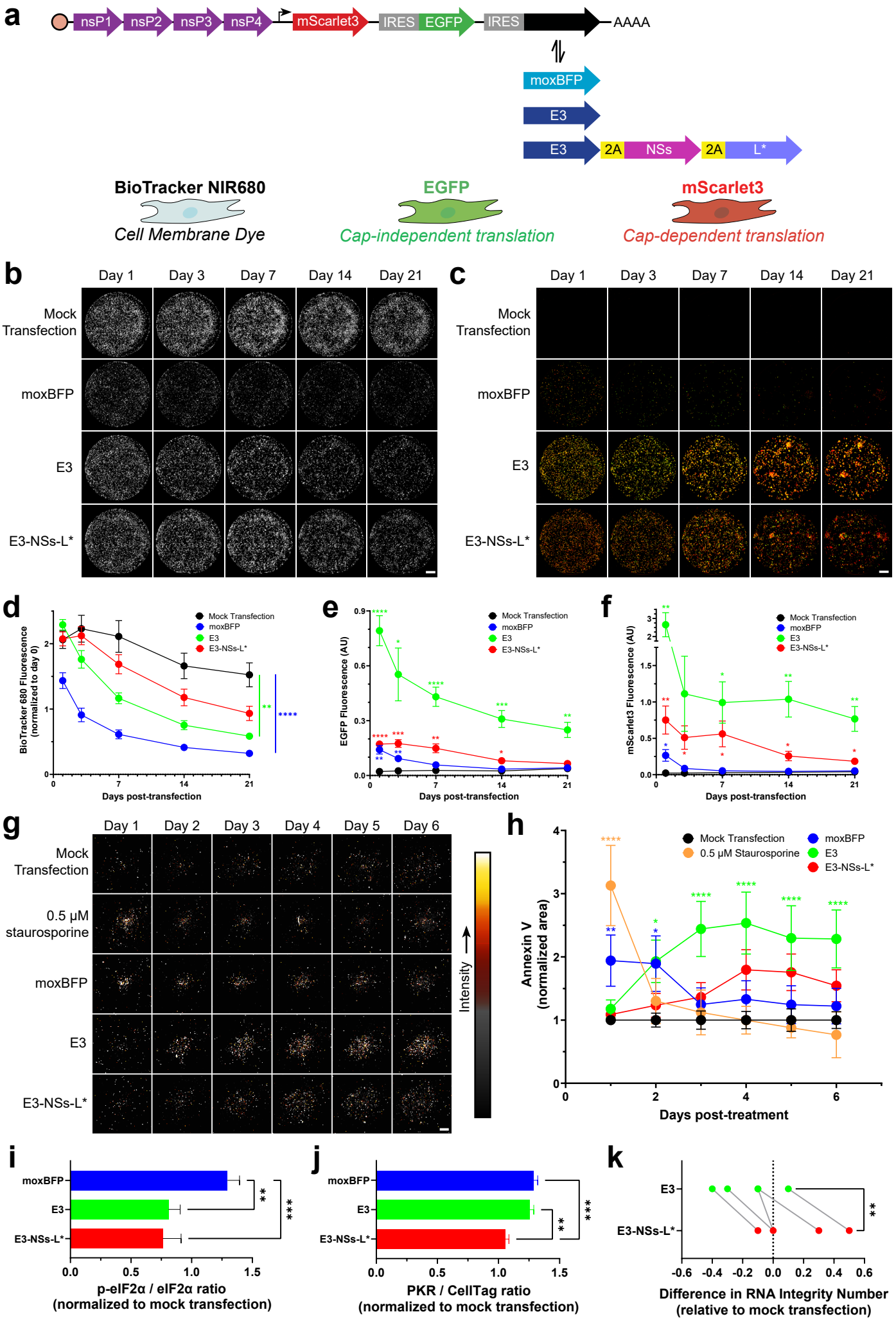
a
nsP1
nsP2
nsP3
nsP4
mScarlet3
IRES
EGFP
IRES
AAAA
moxBFP
E3
E3
2A
NSs
2A
L*
BioTracker NIR680
Cell Membrane Dye
EGFP
Cap-independent translation
mScarlet3
Cap-dependent translation
b
Day 1
Day 3
Day 7
Day 14
Day 21
Mock Transfection
moxBFP
E3
E3-NSs-L*
c
Day 1
Day 3
Day 7
Day 14
Day 21
Mock Transfection
moxBFP
E3
E3-NSs-L*
d
BioTracker 680 Fluorescence (normalized to day 0)
Days post-transfection
Mock Transfection
moxBFP
E3
E3-NSs-L*
e
EGFP Fluorescence (AU)
Days post-transfection
Mock Transfection
moxBFP
E3
E3-NSs-L*
f
mScarlet3 Fluorescence (AU)
Days post-transfection
Mock Transfection
moxBFP
E3
E3-NSs-L*
g
Day 1
Day 2
Day 3
Day 4
Day 5
Day 6
Mock Transfection
0.5 μM staurosporine
moxBFP
E3
E3-NSs-L*
Intensity
h
Annexin V (normalized area)
Days post-treatment
Mock Transfection
0.5 μM Staurosporine
moxBFP
E3
E3-NSs-L*
i
moxBFP
E3
E3-NSs-L*
p-eIF2α / eIF2α ratio
(normalized to mock transfection)
j
moxBFP
E3
E3-NSs-L*
PKR / CellTag ratio
(normalized to mock transfection)
k
E3
E3-NSs-L*
Difference in RNA Integrity Number
(relative to mock transfection)

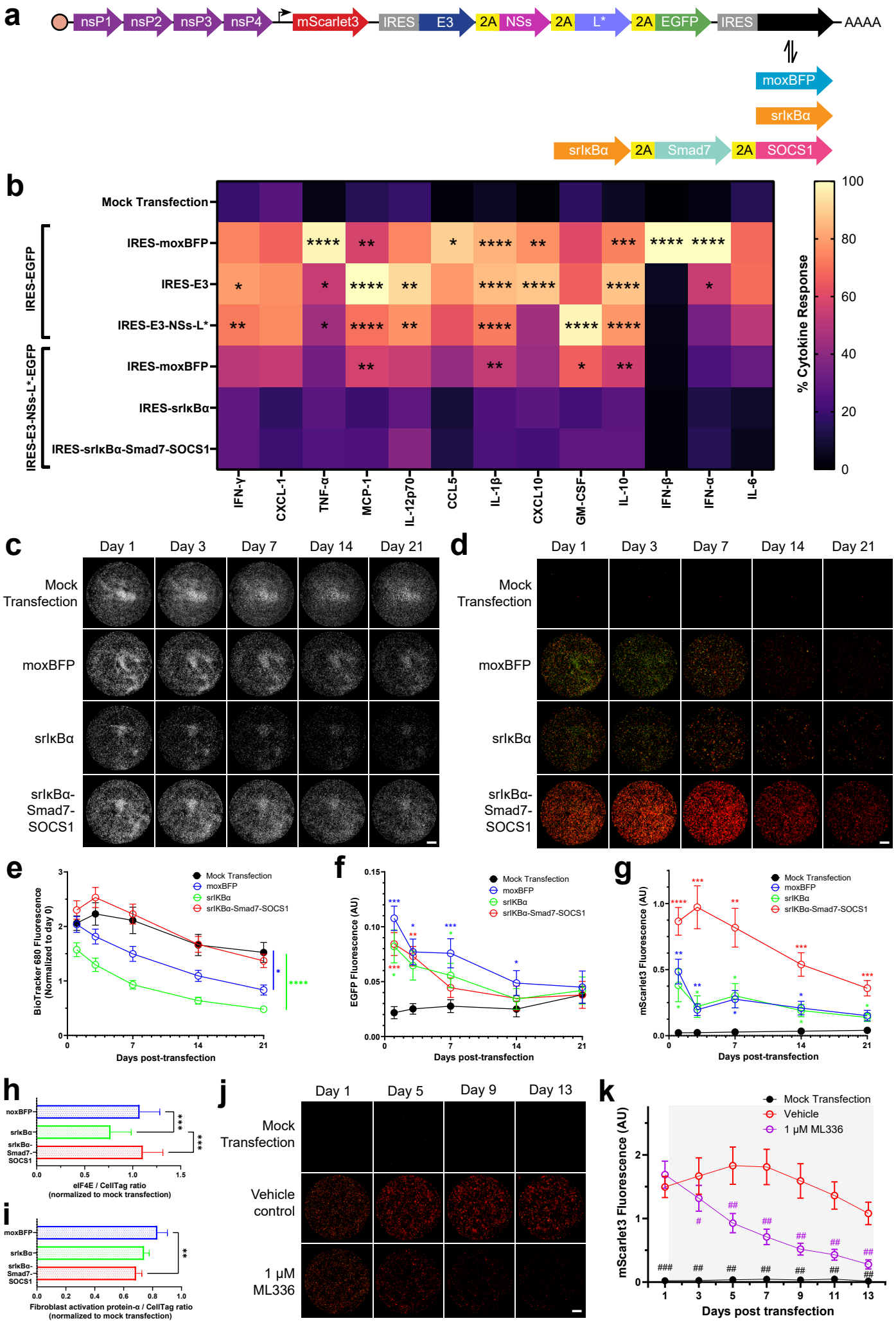
a
nsP1
nsP2
nsP3
nsP4
mScarlet3
IRES
E3
2A
NSs
2A
L*
2A
EGFP
IRES
AAAA
moxBFP
srIκBα
srIκBα
2A
Smad7
2A
SOCS1
b
Mock Transfection
IRES-EGFP
IRES-moxBFP
IRES-E3
IRES-E3-NSs-L*
IRES-E3-NSs-L*-EGFP
IRES-moxBFP
IRES-srIκBα
IRES-srIκBα-Smad7-SOCS1
IFN-γ
CXCL-1
TNF-α
MCP-1
IL-12p70
CCL5
IL-1β
CXCL10
GM-CSF
IL-10
IFN-β
IFN-α
IL-6
% Cytokine Response
100
80
60
40
20
0
c
Day 1
Day 3
Day 7
Day 14
Day 21
Mock Transfection
moxBFP
srIκBα
srIκBα-Smad7-SOCS1
d
Day 1
Day 3
Day 7
Day 14
Day 21
Mock Transfection
moxBFP
srIκBα
srIκBα-Smad7-SOCS1
e
BioTracker 680 Fluorescence (Normalized to day 0)
Days post-transfection
Mock Transfection
moxBFP
srIKBα
srIKBα-Smad7-SOCS1
f
EGFP Fluorescence (AU)
Days post-transfection
Mock Transfection
moxBFP
srIKBα
srIKBα-Smad7-SOCS1
g
mScarlet3 Fluorescence (AU)
Days post-transfection
Mock Transfection
moxBFP
srIKBα
srIKBα-Smad7-SOCS1
h
noxBFP
srIκBα
srIκBα-Smad7-SOCS1
eIF4E / CellTag ratio (normalized to mock transfection)
i
moxBFP
srIκBα
srIκBα-Smad7-SOCS1
Fibroblast activation protein-α / CellTag ratio (normalized to mock transfection)
j
Day 1
Day 5
Day 9
Day 13
Mock Transfection
Vehicle control
1 μM ML336
k
Mock Transfection
Vehicle
1 μM ML336
mScarlet3 Fluorescence (AU)
Days post transfection